

A Methodology considerations

The modeling is separated into capture and mineralization segments.

A.1 Capture

The flue gas generated from industrial processes undergoes a CO₂ separation stage. Mature post-combustion carbon capture mainly relies on wet scrubbers using MEA, given its high reactivity toward CO₂ and low cost.¹ Figure A.1 is a schematic representation of the model developed in Aspen Hysys. The CO₂ capture process is known to be energetically penalizing (Table B.4). Therefore, a good heat integration strategy is also vital to promote its industrial use.

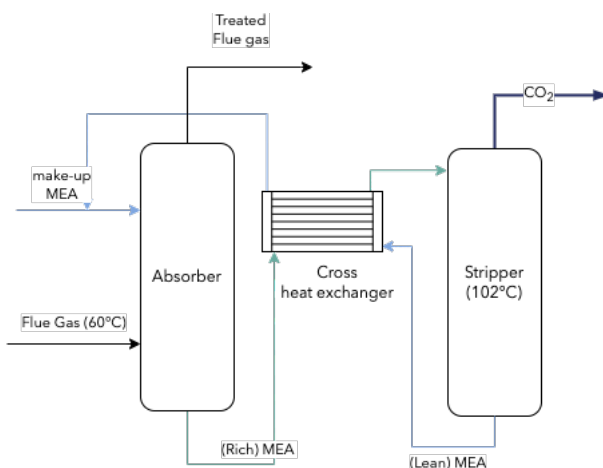


Figure A.1: CO₂ Capture process using an MEA scrubber based on the work of Tock et al.¹ The flue gas enters the bottom of an absorption column at approximately 60 °C, counter-current to the MEA solvent. A selective exothermic reaction occurs between MEA and CO₂. The saturated solution is heated up and fed to the top of a stripping column at T = 102 °C where the recovery of used MEA solvent and the break up of chemical bounds take place. The captured CO₂ leaves from the top stage and the lean solvent closes the solvent loop.

A.2 Mineralization modeling

The choice among direct and indirect carbonation is a trade-off. On the one hand, DC requires the control of dissolution and precipitation in a single reactor, which is often a problem given that both stages have different preferential conditions. However, it entails lower investment and operating costs. On the other hand, IC allows tight control of both steps (thus improved kinetics) albeit a more expensive design. Romanov et al.² provided a good overview of both.

To date, the precise mechanism by which the carbonation reaction proceeds is unclear,³ possibly due to numerous intermediate compounds and side reactions. A tentative mechanism was explored by Pan et al.⁴ and comprises of: (i) CO₂ dissolution and deprotonation, according to Equation 1a-c; (ii) intermediate formation or hydration (Equation 2a) and solubility equilibrium (Equation 2b); (iii) nucleation and precipitation, either via the intermediate (Equation 3a), or the hydroxide (Equation 3 b-c).



The reaction kinetics, *i.e.* which reactions take place and how fast, depend on numerous parameters including particle size, reaction temperature and pressure, liquid-to-solid ratio, chemical additives, and reactor design. A detailed kinetic study is outside the scope of this work; the primary focus is on thermodynamic considerations and operating conditions that ensure kinetic feasibility, and not on optimizing those conditions. However, among kinetic parameters, temperature and chemical additives were particularly significant and taken into account. Although high values are known to accelerate the reaction, the temperature was kept between 80°C and 280°C as suggested by Snaebjornsdottir et al.,⁵ to ensure spontaneous carbonate precipitation (Figure A.2), and avoid side reactions.

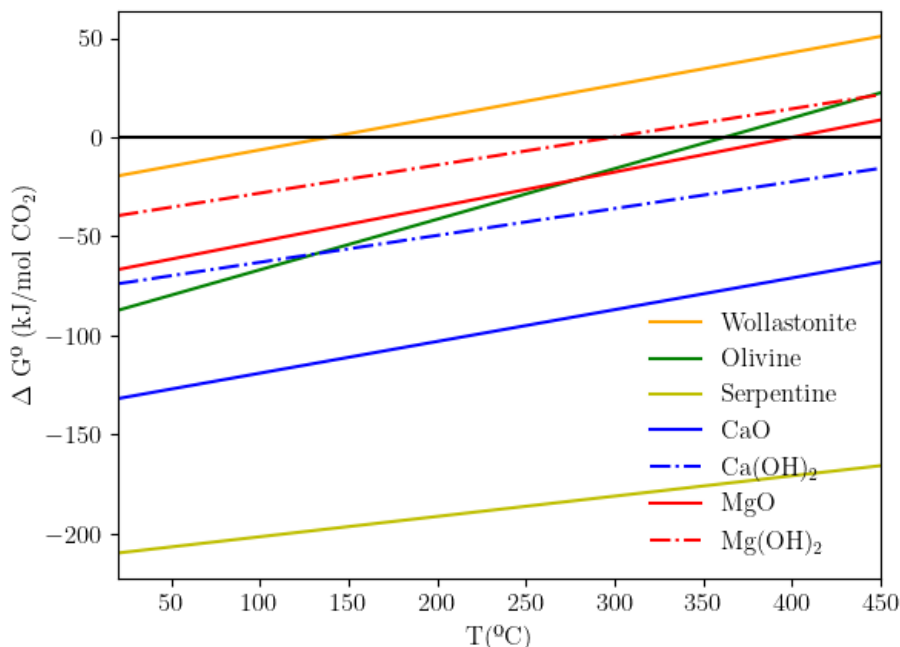


Figure A.2: Gibbs free energy as a function of temperature for mineral ores and intermediates after extraction step. Values below zero identify spontaneous reactions.

A.3 Direct Carbonation

Direct carbonation is a one-step reaction. It shows higher conversion rate and sequestration capacity compared to the indirect option, despite lower value-added product purity,⁶ which might jeopardize process economics.

Mineral ores require mining and transportation to the plant location where the pre-treatment takes place, comprising magnetic separation, grinding, and chemical treatment, with the latter requiring harsh conditions (temperature, pressure, and additives). Reducing the particle size (thus increasing surface area and carbonation rate) to between 10 and 38 μm in the direct carbonation pathway has shown to increase the reaction conversion from 10 to 90%.⁷⁻⁹ According to Huijgen et al.,⁷ Ball and SMD mill grinding are considered to be the most economically and energetically feasible given the large quantities of minerals needed for the sequestration stage. A summary is provided in Appendix A.4.

The powdered feedstock is then brought to the reaction temperature and supplied to the reactor, where it is mixed with aqueous solutions (0.64 M NaHCO_3 and 1 M NaCl). The reactor operating conditions are given in Table A.1 and solvent recovery is assumed to be 90%. The CO_2 captured from the MEA stage is compressed and injected into the reactor. The formed products are transferred to a post-processing step where they are separated, dried, and ready to be discharged or sold based on market specifications.

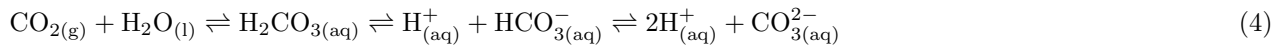
Wollastonite and Olivine have identical pre-treatment procedures. However, the serpentine heat activation procedure is more demanding. After the magnetic separation of Fe_2O_3 , a heat treatment at 600 $^\circ\text{C}$ is required to ensure

fast reaction kinetics. This stage partially dehydroxylates serpentine, modifying its structure and leading to an amorphous material that is more reactive.¹⁰

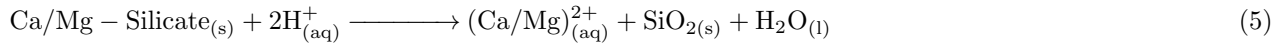
Table A.1: Operating conditions of direct mineralization pathways, based on the work of Gerdemann et al.¹⁰

Minerals	Temperature [°C]	Pressure [MPa]
Olivine	185	15
Serpentine	155	14
Wollastonite	100	4

Direct carbonation consists of a one-step process, comprising several reactions and operations: (i) CO₂ dissolving in water to form bicarbonate (H₂CO₃) and hydrogen ions (H⁺):



(ii) Ca and Mg silicate leach from the mineral matrix,⁷ facilitated by the produced H⁺ ions:



(iii) magnesium and/or calcium carbonate precipitation:⁹



Aspen modeling

Figure A.3 shows the process modeled in Aspen. It comprises three sections: material preparation/pre-treatment (green), reaction and recycling (blue), and solid separation (brown). The following calculation blocks were used:

- WATERIN: Defines the amount of make-up water (WATER stream) that enters the mixer M2, according to a Solid-to-Liquid ratio of 0.15¹⁰ and the recycled amount from stream H2O.

- FEEDIN: Computes the amount of either calcium silicate (CaSilic) or magnesium silicate (MgSilic) that needs to enter to fully mineralize the amount of CO₂ entering in CO2IN.
- CO2FLOWI: Imposes a discharging pressure and temperature of CO2 in CO2PRESS compatible with REACTOR conditions.
- RTP: Defines the pressure elevation in PUMP and the heat required to bring ALKMIX to the REACTOR temperature and pressure.
- C-1 and C-2: Computes the conversion (Tear variable) of the magnesium (C-1) and calcium (C-2) fractions as a function of reactor temperature and pressure.

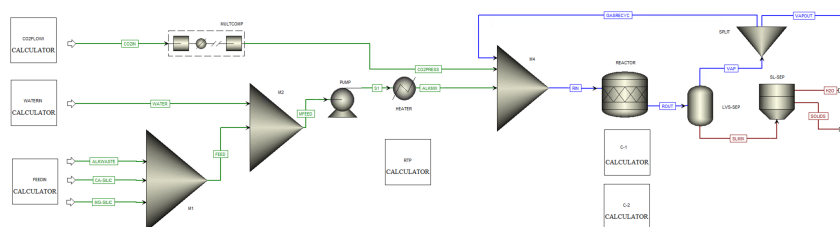


Figure A.3: Direct Carbonation model

The REACTOR is modeled as an RStoic with the conversion for each fraction computed in calculator nodes C-1 and C-2. Kinetic experiments¹⁰ on Ca and Mg silicates suggest operating conditions for Olivine (185°C and 150 bar), Serpentine (155°C and 115 bar), and Wollastonite (100°C and 40 bar). Semi-empirical correlations were deduced from the same reference to model both C-1 and C-2 calculators, by linearizing the effect of both temperature and pressure on mineral conversion. The triphasic mixture (ROUT) is separated in the LVS-SEP separator; 90% of the gas stream is recycled back to the reactor (GASRECYC). The solid/liquid mixture (SLMIX) is further separated in SL-SEP, achieving a solid with 0.15 residual humidity (dry basis).⁷ The liquid stream (H2O) is recycled back to M2.

Mass and energy requirements

This section summarizes in the form of a flowsheet the different mass and energy requirements for each pathway. Electricity values are highlighted in blue, whereas red boxes refer to heat supply or demand (depending on the direction of the arrow). The quality of the heat – given by its temperature level – is next to the red boxes. Values between brackets correspond to the amount of heat between those temperatures.

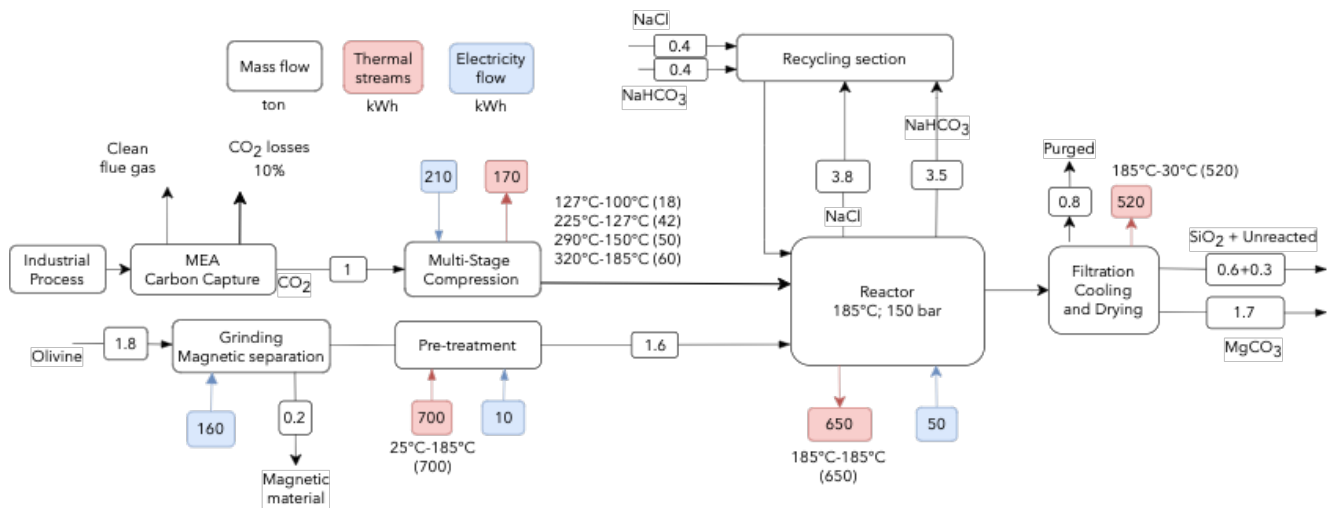


Figure A.4: Flowsheet of olivine direct carbonation.

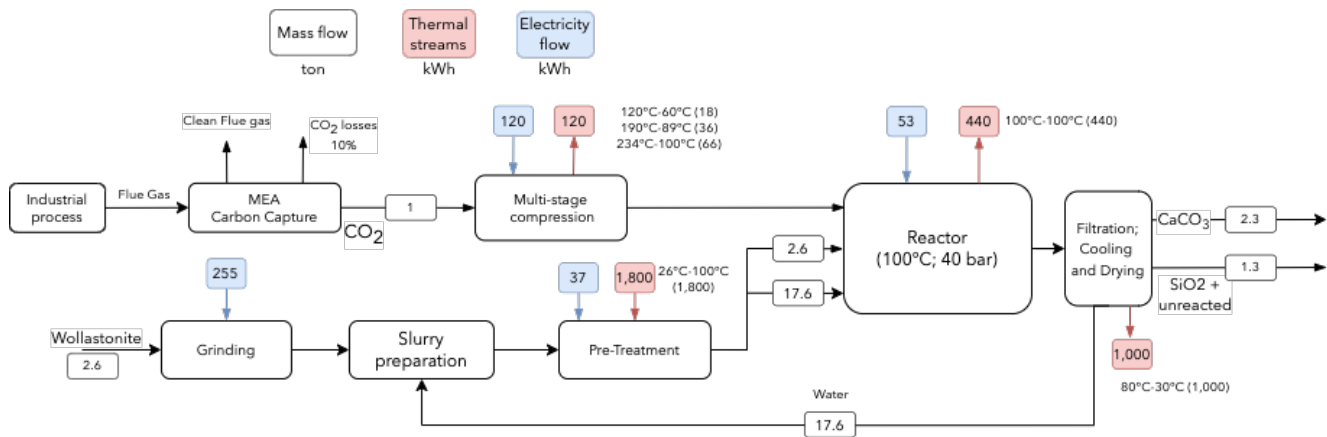


Figure A.5: Flowsheet of the direct carbonation of wollastonite.

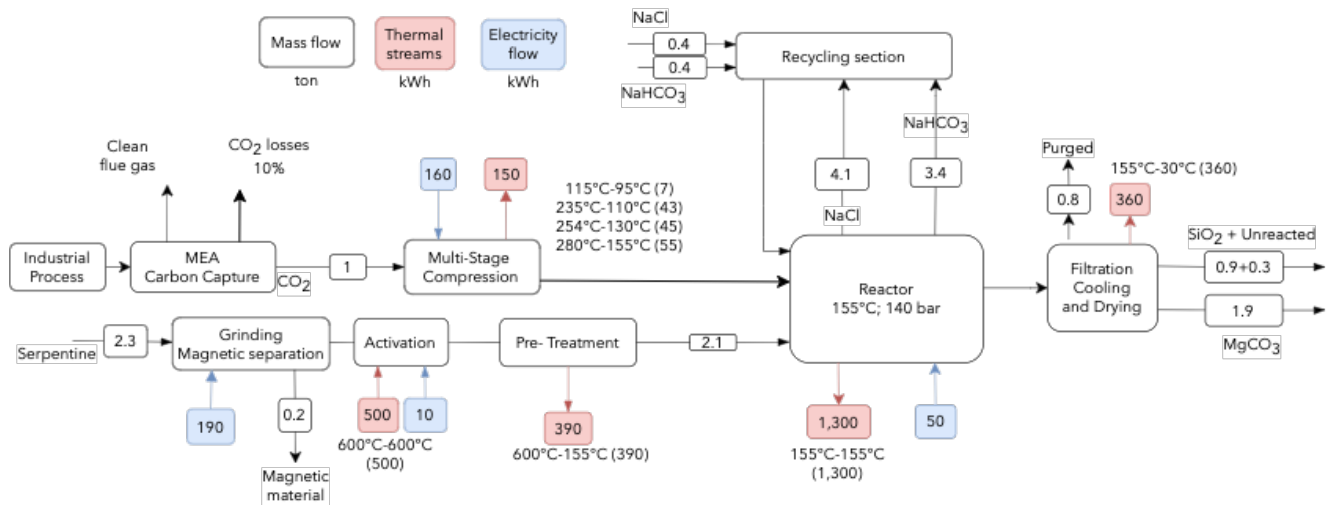


Figure A.6: Flowsheet of the direct carbonation of serpentine.

A.4 Indirect Carbonation

IC is a multi-step process (Figure A.7), more complex and requiring more control *vis-à-vis* the direct option. Operating conditions depend on feedstock and leaching agent as summarized by Zhang et al.¹¹ Compared to direct carbonation, it leads to higher carbonate purity (as impurities are previously separated), which is useful in a wide range of downstream applications. Separating the process is also a way to promote kinetically faster steps.² IC operates at higher temperatures,^{2,11} thus achieving higher leaching efficiency.¹² In this work, only serpentine and wollastonite were used. The indirect carbonation of olivine was only barely studied and showed considerably lower conversion efficiencies.¹¹ It was therefore discarded.

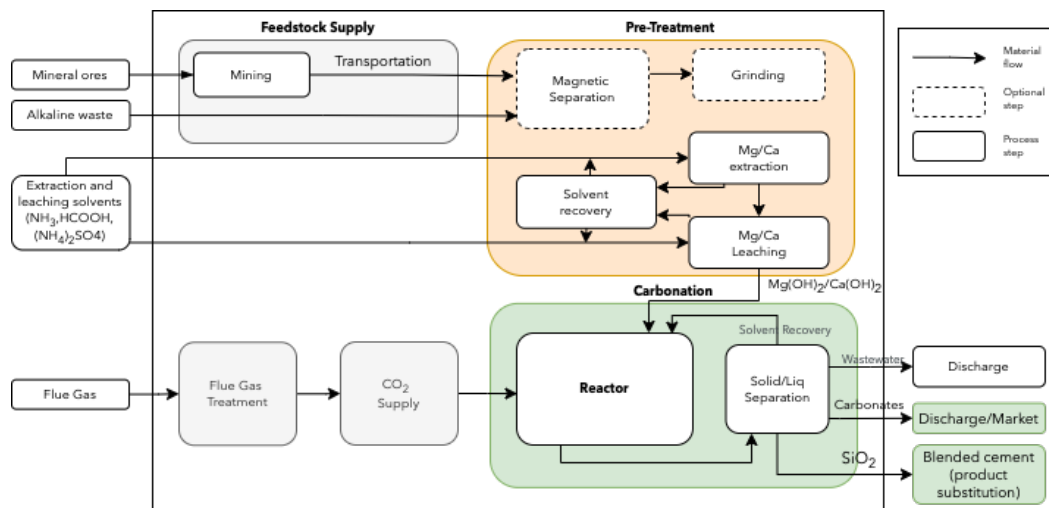


Figure A.7: Indirect mineralization system boundaries. Mineral ores refer to naturally-occurring and exploitable magnesium and calcium sources (serpentine and wollastonite). Extraction treatment is dependent on the type of mineral ore and leaching metal.

Wollastonite (a calcium-based silicate) has shown more reactive kinetics than magnesium silicates,¹³ reaching at least 70% extraction in under one hour.¹⁰ The calcium silicate used is pristine wollastonite, with 90% purity and chemical composition: SiO₂ 51.71 wt%, CaO 46.06 wt%, Fe₂O₃ 0.41 wt%, Al₂O₃ 0.41 wt%, MgO 1.16 wt%. It is ground to $\leq 20 \mu\text{m}$ to ensure fast reaction kinetics using a ball mill. A leaching rate of 85.7% occurs at 80 °C using formic acid, followed by precipitation of calcium hydroxide. This active compound reacts at 300°C and calcium carbonate precipitates. The solids are then washed and dried.

For serpentine, the first step is again the leaching process, which extracts the metal ion from the solid matrix. The protocol described by Fagerlund et al.¹⁴ was adopted, using ammonium sulfate as a leaching agent. In the second step, by means of increasing pH – commonly known as ‘pH swing’ – selective precipitation occurs, using NH₄OH as a pH regulator. The third step is the carbonation reaction itself. According to Fagerlund et al.¹⁴ the reactivity of the leached compound (Mg(OH)₂ or Ca(OH)₂) is better than any mineral ore of oxide (MgO or CaO), thus justifying the previous leaching and precipitation step.

In the indirect carbonation procedure, the extraction of magnesium and/or calcium from their silicates matrix precedes the carbonation reaction. This extraction can be done either using acids or bases.¹¹ Acids were selected, given their predominance among experimental studies, albeit some concerns related to separation and reuse.¹¹ The added complexity to this route, compared to the direct carbonation one, allows for better control of particle size and morphology, promoting the nucleation and growth of carbonation products of higher purity.¹⁵ On the scalability side, solvent recovery is an essential step. The presence of multiple compounds and phases makes it particularly challenging.⁷ Modeling and simulation were broken into stages.

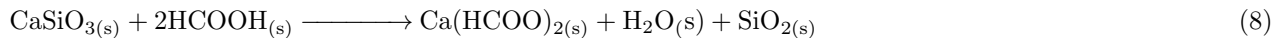
Stage I

It represents the use of weak acids for the extraction of minerals from their silicate matrix, concerning calcium, magnesium, and aluminum. The rate-limiting step of the leaching process is related to product layer diffusion, justifying low Solid-to-liquid ratios and high-speed agitation, promoting a more intimate contact between solid and extraction solution.

Magnesium Extraction The Abo Academy process, which suggests a staged process for the magnesium silicate carbonation, is partially followed in this work. In its first step, the Mg compound is extracted from the magnesium silicate (of serpentine) using Ammonium Sulfate, (NH₄)₂SO₄, acting as a weak acid^{16,17} in the form of magnesium sulfate (MgSO₄), according to Equation 7. As reported by Romao et al.,¹² the formed MgSO₄ cannot be directly converted to MgCO₃, as it is thermodynamically unfavorable.



Calcium Extraction Different acids are possible for extraction: acetic acid, formic acid, and lactic acid. Although all show non-corrosive performance,⁷ their recycling is the main operating constraint. Formic acid is selected as it shows the best kinetics, extracting 96% of Ca in Wollastonite at 80°C.¹⁸



Stage II

The hydroxide formation step, via precipitation, is the main intermediate connecting the extraction and the carbonation stages.

Magnesium Hydroxide NH_3 and H_2O produced in the first Mg extraction stage react in their vapor phase to produce Ammonium Hydroxide (NH_4OH) in the Gibbs-type reactor and establish an equilibrium:



The produced NH_4OH is then responsible for the precipitation of the hydroxide, in a process commonly known as 'pH-swing'. Simultaneously, the sulfate is regenerated and recycled to Stage I.



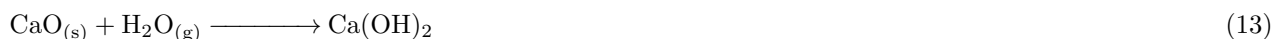
However, this extraction reaction (Equation 10) lacks kinetic data. For instance, the Abo Academy procedure handled it as an equilibrium reactor, achieving full conversion at high operating temperature and pressure.¹⁹ In this work, the kinetics of the reaction were modeled instead using a CSTR and kinetics of $\text{Mg}(\text{OH})_2$ formation in water instead of NH_4OH :



Calcium Hydroxide Formation The extracted $\text{Ca}(\text{HCOO})_2$ reacts with water leading to the formation of $\text{Ca}(\text{OH})_2$ necessary for the CaCO_3 formation:



Since insufficient kinetics data were found regarding the Calcium Hydroxide $\text{Ca}(\text{OH})_2$ formation from $\text{Ca}(\text{HCOO})_2$, kinetics data using Calcium oxide (CaO) as a reactant, which is believed to be the main intermediate, were used instead (Equation 13).



The reaction rate is assumed to follow an Arrhenius type (Equation 14) with the reference rate (k) = $2.5 \cdot 10^{-6} \text{ s}^{-1}$, the activation energy (E_a) = $5.7 \cdot 10^4 \frac{\text{J}}{\text{mol}}$ and the reference temperature (T_0) = 1073 K, with T the reaction temperature, and R the ideal gas constant.

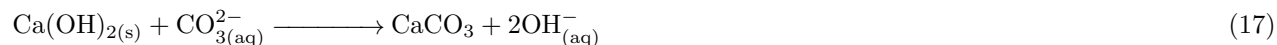
$$\text{rate} = k \cdot e^{-\frac{E_a}{R} \left(\frac{1}{T} - \frac{1}{T_0} \right)} \quad (14)$$

Stage III

Magnesium Carbonate Formation $\text{Mg}(\text{OH})_2$ reactivity with CO_2 is considerably better in comparison with magnesium silicates or MgO .¹⁹ At ambient temperature, the reaction is slow but increases significantly with temperature. The carbonation reactor conditions were chosen at 300 °C and 25 bar.¹⁹



Calcium Carbonate Formation Similarly to the carbonation of magnesium, $\text{Ca}(\text{OH})_2$ reacts and forms carbonates:



The reaction operates at 300 °C and 1 MPa, and follows an Arrhenius law, with a reaction rate constant $k = 0.5 \text{ h}^{-1}$ and activation energy $E_a = 7.5 \frac{\text{kJ}}{\text{mol}}$.

Aspen modeling

Figure A.8 shows the modeling of the indirect carbonation procedure. The flowsheet is broken into three sections, corresponding to each of the stages previously described. Green color corresponds to the extraction stage (stage I); blue color to the hydroxide formation (stage II); brown streams correspond to the final stage of carbonation and separation (stage III). Thermodynamic properties are based on the Peng-Robison equation of state; precipitated/solid compounds are declared in the properties section and the SOLIDS thermodynamic method is used whenever these compounds are present.

- FEEDIN: Computes the amount of either calcium silicate (CaSilic) or magnesium silicate (MgSilic) that needs to enter to fully mineralize the amount of CO₂ entering in CO2IN. In addition, the amount of water, formic acid, ammonium bisulfate, and ammonia is computed, as a function of inlet CO₂.
- STAGE1TP: Defines the pressure elevation in PUMP1 and the heat required to bring MFEED to the REACTOR1 temperature and pressure.
- 2-1TP: Imposes the operation of HEATER2 and HEATER4 to reach temperature conditions of STAGE2-1 reactor conditions
- 3-1TP: Imposes the operation of HEATER6, PUMP2 and COMP2 to reach temperature and pressure conditions adequate to STAGE3-1 reactor.
- 3-2TP: Imposes the operation of HEATER8, PUMP3 and COMP3 to reach temperature and pressure conditions adequate to STAGE3-2 reactor.

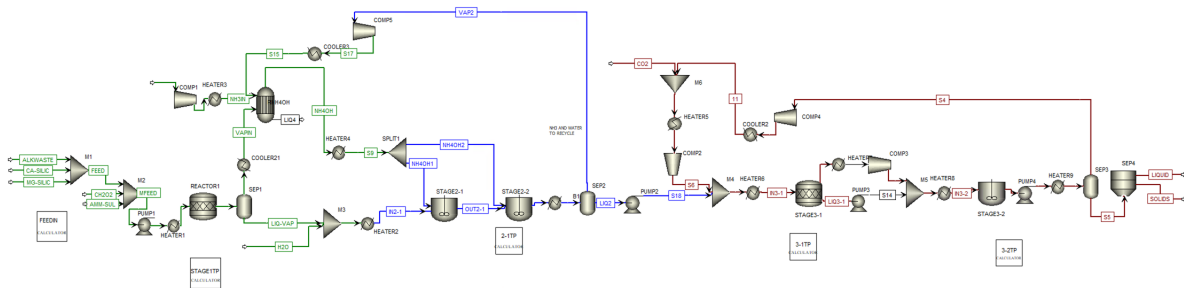


Figure A.8: Indirect Carbonation model.

In Aspen Plus model, the first step is modeled as a stoichiometric reactor operating at 400 °C and 5 bar; the NH₄OH production reactor (RNH4OH) is modeled as a Gibbs reactor; the precipitation of the Mg(OH)₂ (idem for Ca(OH)₂), follows a pH-swing procedure, modeled as two CSTR. Captured CO₂ is compressed, and then mixed with

the products from stage II. According to Fagerlund et al.,¹⁴ the formation of carbonates from $Mg(OH)_2$ depends on ratio between water and CO_2 (p_{H_2O}/p_{CO_2}). The carbonation reaction is favored at 300 °C and 25 bar, and a pressure ratio of 14.4. Several reactions take place in the carbonation stage, one of which is the $Mg(OH)_2$ dehydroxilation to MgO . Such side reactions can be tuned to promote its reaction with CO_3^{2-} and produce $MgCO_3$.¹⁴ This step should take place in a fluidized bed reactor due to the range of operating conditions; it is modeled as an RTSOIC reactor with an average reaction conversion of 60%. The calcium reaction follows an identical procedure, achieving 77% conversion.

Mass, Energy and Thermal requirements

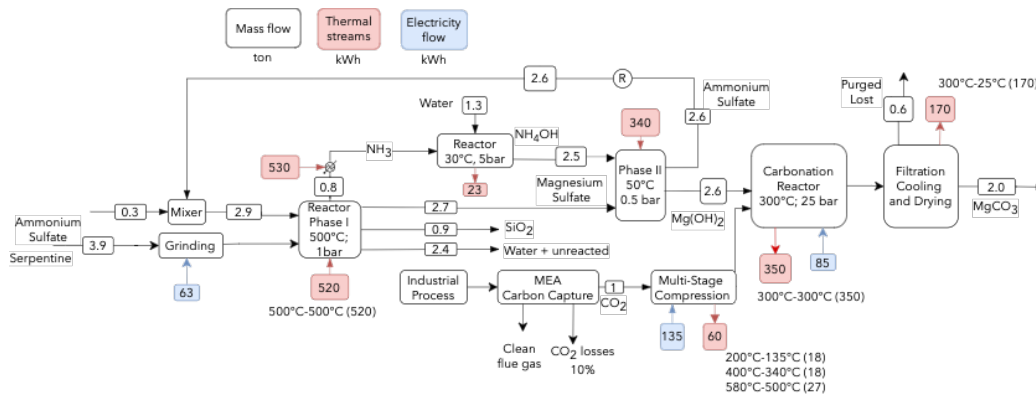


Figure A.9: Flowsheet of serpentine indirect carbonation.

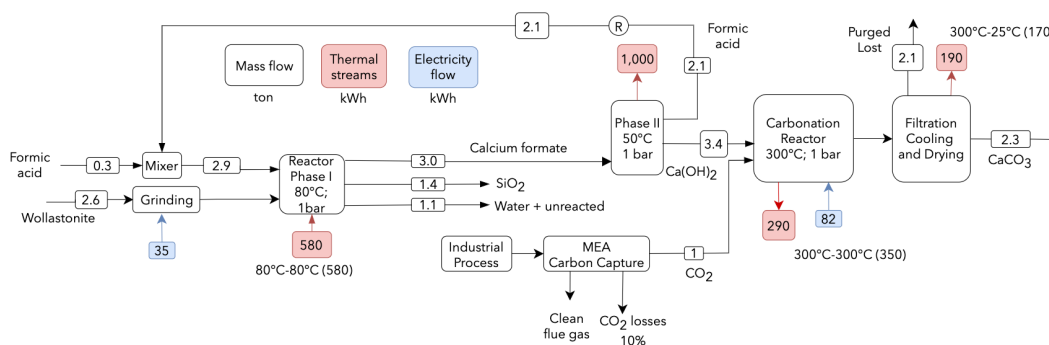


Figure A.10: Flowsheet of wollastonite indirect carbonation.

Pre-treatment

Crushing and grinding to the desired particle size is a crucial step in pre-treatment with significant electricity consumption (Table A.2). It is more relevant in direct carbonation, with ideal particle size below 10 μm ,⁸ whereas in indirect carbonation, particle size up to 425 μm is adequate.¹⁴ In this work, the summary values provided by⁷ were used. Serpentine is, among the ultramafic rocks, the one in need of harsher conditions, including high-temperature heat, required to remove chemically bounded water.

Table A.2: Size reduction pre-treatment of minerals.²⁰ SMD: stirred media detritor.

Mineral	Grinding method	Electricity consumption (kWh/ton)	Heat treatment (kWh/ton)
DC - Olivine	SMD Mill ($\leq 10 \mu\text{m}$)	233	–
DC - Serpentine	Ball Mill ($\approx 38 \mu\text{m}$)	83	293 (@630°C)
DC - Wollastonite	SMD Mill ($\leq 10 \mu\text{m}$)	167	–
IC - Serpentine	Ball Mill ($\approx 75 \mu\text{m}$)	13	293 (@630°C)
IC - Wollastonite	Ball Mill ($\approx 20 \mu\text{m}$)	97	–

A.5 Mathematical formulation

The solution generation strategy contains three main blocks to generate industrial designs. The Total Cost (TC) of the process is minimized by computing thermodynamically feasible energy targets. The problem is solved using a MILP formulation, as it is able to capture the binary and continuous behavior of the system. Binary variables (y_u) are used for unit selection and continuous variables (f_u) for unit size.

Energy integration model

The PI model is based on mass and energy balances, as well as heat cascade equations. Supply and demand (of any type of resource) are modeled using units. The system includes two types: process units ($pu \in \mathbf{PU}$), and new units ($nu \in \mathbf{NU}$). Process units represent a default industrial production and are imposed with a fixed size. On the other hand, new units are employed to satisfy requirements (from process units) and can be sized accordingly; they are not in place and require investment.

The approach featured in Maréchal and Kalitventzeff²¹ and based on the work of Linnhoff and Hindmarsh²² is used to satisfy the minimum energy requirements, combining heat cascade with pinch analysis to obtain the optimal utility network, with minimal cost. For each temperature level k the energy balance is closed (Equation 18), with heat flowing from higher (k) to lower ($k - 1$) temperature levels. Thermodynamic feasibility is ensured by positive heat flows (Equation 19) and zero flow in both the first and last temperature intervals (Equation 20)

Constraints are placed on the minimum (f_u^{\min}) and maximum (f_u^{\max}) capacity of each unit (Equation 21). Moreover, each unit u supplies and requires resources, given by $\dot{m}_{r,u}^+$ and $\dot{m}_{r,u}^-$, respectively. The overall supply and consumption of a unit is given by Equation 22 and Equation 23, respectively. The overall resource balance is closed, according to Equation 24. An extra triple index variable ($\dot{x}_{r,i,j}$) is defined to account for exchanges between units, according to Equation 25. Lastly, to enforce that units can only exchange what they are able to supply, Equation 26 is added.

Heat cascade constraints: $\forall k \in \mathbf{K}$ with $T_{k+1} \geq T_k$

$$\sum_{u \in \mathbf{U}} \dot{q}_{u,k} \cdot f_u + \dot{R}_{k-1} - \dot{R}_k = 0 \quad (18)$$

$$\dot{R}_k \geq 0 \quad (19)$$

$$\dot{R}_0 = \dot{R}_{k+1} = 0 \quad (20)$$

Resource and size constraints:

$$f_u^{\min} y_u \leq f_u \leq f_u^{\max} y_u \quad \forall u \in \mathbf{U} \quad (21)$$

$$\dot{M}_{r,u}^+ = \dot{m}_{r,u}^+ \cdot f_u \quad \forall r \in \mathbf{R}, \forall u \in \mathbf{U} \quad (22)$$

$$\dot{M}_{r,u}^- = \dot{m}_{r,u}^- \cdot f_u \quad \forall r \in \mathbf{R}, \forall u \in \mathbf{U} \quad (23)$$

$$\sum_{u \in \mathbf{U}} \dot{M}_{r,u}^+ = \sum_{u \in \mathbf{U}} \dot{M}_{r,u}^- \quad \forall r \in \mathbf{R} \quad (24)$$

$$\dot{M}_{r,u}^+ + \sum_{\substack{i \in \mathbf{U} \\ i \neq u}} \dot{x}_{r,i,u} = \dot{M}_{r,u}^- + \sum_{\substack{j \in \mathbf{U} \\ j \neq u}} \dot{x}_{r,u,j} \quad \forall r \in \mathbf{R}, \forall u \in \mathbf{U} \quad (25)$$

$$\sum_{\substack{i \in \mathbf{U} \\ i \neq u}} \dot{x}_{r,u,i} \leq \dot{M}_{r,u}^+ \quad \forall r \in \mathbf{R}, \forall u \in \mathbf{U} \quad (26)$$

Economic model

The economic model links the PI stage with monetary flows and is used to compute the total cost of the system, composed of investment (Capex) and operating expenses (Opex). The operating cost of the different units (new and process) is computed according to Equation 27 and accounts for both fixed (e.g. maintenance) and variable costs, associated with the activation and size of the units, respectively. c_u^{op1} and c_u^{op2} are fixed and variable operating costs. Δt^{op} is the operating time (8,000 hours per year).

$$\text{Opex} = \sum_{u \in \mathbf{U}} \left(c_u \cdot y_u + c_u^{op2} \cdot f_u \right) \cdot \Delta t^{op} \quad (27)$$

According to Turton,²³ the investment cost of a unit is not only its purchasing cost (C_u^b), but also materials (e.g. fittings), labor, freight, overhead, and engineering costs. Equation 28 calculates the total investment cost, where F_u^{mt} , F_u^{lr} , F_u^{fr} , F_u^{oh} , F_u^{en} are cost factors (fractions of the purchase cost adapted from²³) for material, labour, freight, overhead, and engineering, respectively. The cost is annualized using the interest rate (i) and the expected project lifetime (n).

$$\text{Capex} = \sum_{u \in \mathbf{NU}} \left[C_u^b \cdot \left(1 + F_u^{mt} + F_u^{lr} + F_u^{fr} + F_u^{oh} + F_u^{en} \right) \right] \cdot \frac{i \cdot (1+i)^n}{(1+i)^n - 1} \quad (28)$$

Purchase cost is calculated based on the investment decisions y_u and f_u in Equation 29. c_u^{inv1} and c_u^{inv2} are fixed and variable investment cost parameters related to the existence and size of the units, respectively. Such parameters are derived using equipment cost functions (detailed in Appendix C).

$$C_u^b = c_u^{inv1} \cdot y_u + c_u^{inv2} \cdot f_u \quad \forall u \in \mathbf{NU} \quad (29)$$

Through optimization, the integration of CCS engenders a different use of heat within the industrial sector. This implies a different ‘interface signature’, with changes in the heat exchanger network. This results in a HEN superstructure optimization and a NLP formulation, which is outside the scope of this work. However, the energy integration formulation allows for estimating both the HEN area, and the number of heat exchangers.²⁴ The details of such a post-computational method based on the final temperature-enthalpy profile are described in Appendix C.1.

LCA model

The carbon footprint is given by Equation 30. From an environmental perspective, the construction and maintenance (c_u^{imp1}) as well as operation (c_u^{imp2}) of all units is taken into account. An associated LCIA Ecoinvent profile is linked to the model. Appendix B summarizes the costs and environmental assessment indicators used.

$$\text{Carbon footprint} = \sum_{u \in \mathbf{U}} (c_u^{imp1} \cdot y_u + c_u^{imp2} \cdot f_u) \cdot \Delta t^{op} \quad (30)$$

A.6 Energy mix evolution

The penetration of VRE is expected to progressively reduce the equivalent carbon content of electricity, depending on the extent and speed of its deployment. This behavior can be modeled using a logistic function. Such a function was originally intended to describe population growth,²⁵ but quickly found other applications, such as microbial and seed growth or even the model of power curves in wind turbines.²⁶

The same rationale can be applied to the grid carbon content as a function of time, by choosing the parameters adequately. A three-parameter logistic function is adopted (Equation 31), in which C is the carbon content as a function of time(t), L is the curve’s maximum value, $z0$ is the midpoint and $k0$ is the slope of the curve. Forecasting the evolution of such indicators is not an easy task. It is assumed that the maximum value (L) is 400 gCO₂/kWh, which is in line with average EU values.²⁷ The two remaining parameters were adapted to fit three quantitative speeds of VRE adoption: fast ($k0 = -0.9$; $z0 = 5$), average ($k0 = -0.5$; $z0 = 10$), and slow ($k0 = -0.5$; $z0 = 15$).

$$C(t) = \frac{L}{1 + \exp(-k0 \cdot (t - z0))} \quad (31)$$

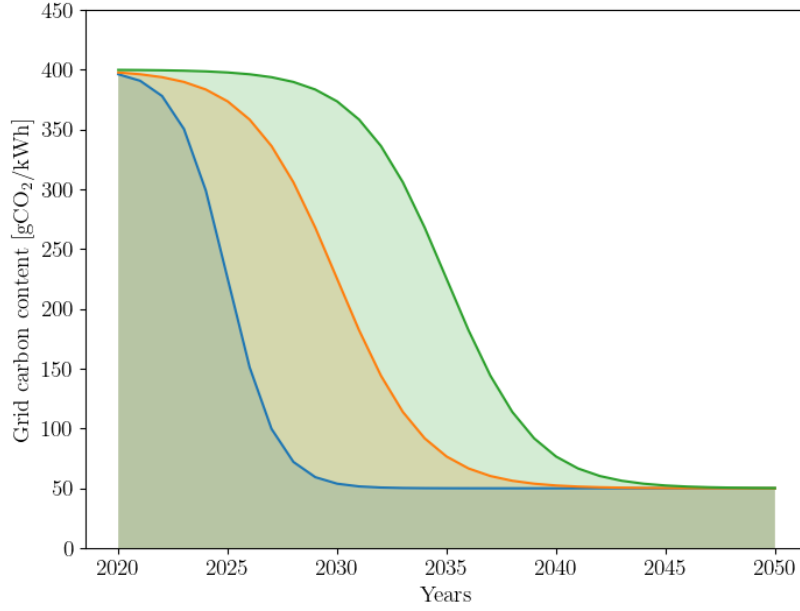


Figure A.11: Logistic function evolution of grid carbon content (C), as a function of time (t), for fast (blue), average (orange) and slow (green) VRE adoption.

With the electricity evolution profiles, the impact of each industrial sector can be assessed as the sum of annual impacts until 2050. The result is the average lifetime impact of each mineralization strategy, according to Equation 32.

$$\overline{\text{Carbon footprint}} = \frac{\int_{t_i=2020}^{t_f=2050} \text{Carbon footprint}(C(t)) dt}{(t_f - t_i)} \quad (32)$$

B Industrial sectors and assumptions

The temperature-enthalpy profile of the cement, MSW and steel sectors are shown in Table B.1, Table B.2, and Table B.3, respectively. The profile for the MEA capture stage is shown in Table B.4. The profile of the considered DHN is provided in Figure B.1, containing the demand per month and the return temperature. The supply temperature (T^{in}) is constant and equal to 60°C all year round. The composition of the alkaline solid residues is provided in Table B.5. Cost assumptions are summarized in Table B.6, whereas environmental indicators in Table B.8.

Table B.1: Temperature-enthalpy profile of the cement sector per ton of produced cement.

Streams	T^{in} ($^{\circ}\text{C}$)	T^{out} ($^{\circ}\text{C}$)	h^{in} (kWh/t)	h^{out} (kWh/t)
cement s1	20	585	0	204
cement s2	1995	115	690	0
cement s3	1995	1995	253	0
cement s4	42	61	0	9
cement s5	105	105	0	40
cement s6	23	42	0	9
cement s7	61	78	0	8
cement s8	95	105	0	4
cement s9	78	95	0	8
cement s10	1145	420	300	0
cement s11	995	420	238	0
cement s12	737	905	0	70
cement s13	905	905	0	655
cement s14	905	915	0	3
cement s15	105	481	0	156
cement s16	481	709	0	94
cement s17	105	752	0	268
cement s18	1331	1381	0	14
cement s19	905	905	5	0
cement s20	1231	1331	0	28
cement s21	1078	425	172	0
cement s22	905	905	4	
cement s23	1031	1231	0	55
cement s24	1381	1449	0	19
cement s25	915	915	0	3
cement s26	915	1031	0	32
cement s27	1439	94	355	0
cement s28	25	252	0	60
cement s29	25	1083	0	279

Table B.2: Temperature-enthalpy profile of the waste sector per ton of MSW incinerated.

Streams	T^{in} ($^{\circ}\text{C}$)	T^{out} ($^{\circ}\text{C}$)	h^{in} (kWh/t)	h^{out} (kWh/t)
MSW s1	845	845	1645	0
MSW s2	845	95	1338	0
MSW s3	30	95	0	48
MSW s4	175	67	439	0

Table B.3: Temperature-enthalpy profile of the steel sector per ton of manufactured steel.

Streams	T^{in} ($^{\circ}\text{C}$)	T^{out} ($^{\circ}\text{C}$)	h^{in} (kWh/t)	h^{out} (kWh/t)
steel s1	25	1205	0	539
steel s2	695	15	97	0
steel s3	595	15	97	0
steel s4	1595	1595	484	0
steel s5	1595	115	261	0
steel s6	1095	15	56	0
steel s7	695	15	52	0
steel s8	25	1105	0	346
steel s9	245	15	75	0
steel s10	1595	1595	917	0
steel s11	1595	115	494	0
steel s12	175	15	79	0
steel s13	245	15	79	0
steel s14	1495	15	162	0
steel s15	25	1185	0	443
steel s16	1595	1595	3750	0
steel s17	1595	115	2019	0
steel s18	1695	1195	198	0
steel s19	1195	1195	77	0
steel s20	1195	15	147	0
steel s21	1695	15	27	0
steel s22	1695	15	67	0
steel s23	25	85	0	10
steel s24	75	15	2	0
steel s25	345	15	304	0
steel s26	695	15	252	0
steel s27	25	1305	0	33

Table B.4: Temperature-enthalpy profile of the MEA capture per ton of CO_2 .

Streams	T^{in} ($^{\circ}\text{C}$)	T^{out} ($^{\circ}\text{C}$)	h^{in} (kWh/t)	h^{out} (kWh/t)
MEA s1	105	35	92	0
MEA s2	107	121	0	92
MEA s3	126	128	0	54
MEA s4	47	108	0	843
MEA s5	95	35	123	0

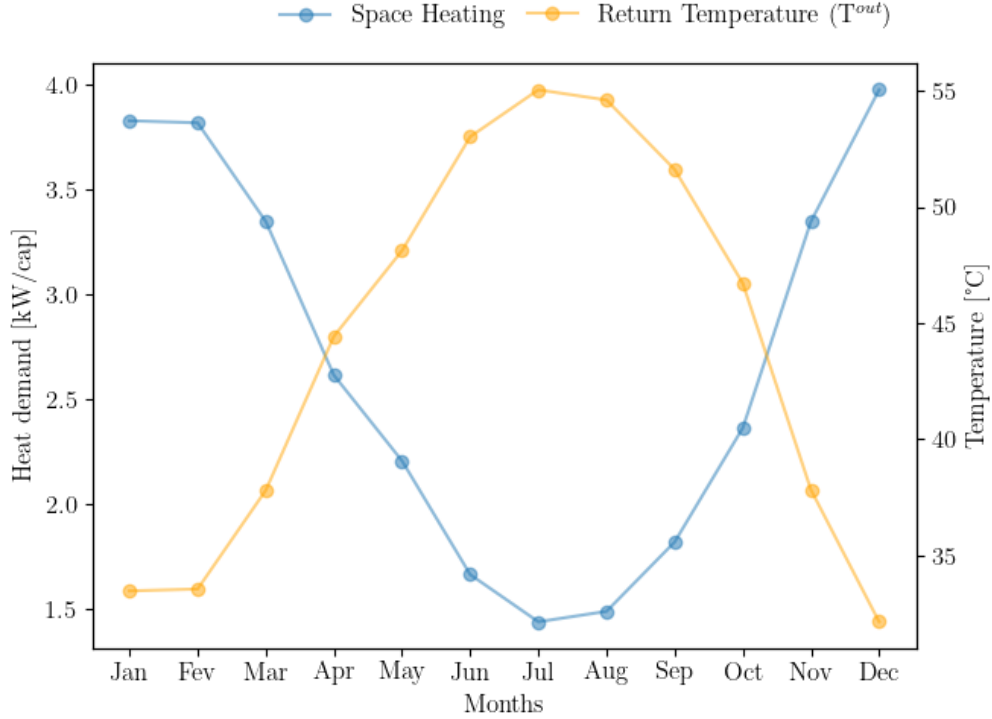


Figure B.1: District heating network demand per month, based on the work by Suciú.²⁸ Constant supply temperature of 60°C, all year round. For formulations with only a time step a weighted average was used instead.

Table B.5: Calcium (CaO) and Magnesium (MgO) mass fraction in different alkali waste streams.

Sector	CaO	MgO	Reference
Waste Incineration	0.19	0.026	90% BA and 10% FA ⁴
Iron and Steel	0.511	0.024	⁴
Cement	0.42	0.018	Cement Kiln Dust ⁴

Table B.6: Feedstock and reactant market prices. Values were updated from 2005 to 2021 using the average annual inflation (2.52%) according to the bureau of labor statistics.

Material	Price (EUR/ton)	Reference
Olivine (Mg_2SiO_4)	31	29
Serpentine ($Mg_3Si_2O_5(OH)_4$)	24	29
Wollastonite ($CaSiO_3$)	24	29
Magnetite (Fe_3O_4)	49	30
NH_3	509	30
$(NH_4)SO_4$	581	30
$NaHCO_3$	367	30
HCOOH (formic acid)	612	30
NaCl	119	30

Table B.7: Economic assumptions using 2021 values for Switzerland.

Parameter	Unit	Value	Reference
Price electricity	[EUR/kWh]	0.041	31
Impact electricity	[kgCO ₂ – eq/kWh]	0.172	31
Price heat (DHN)	[EUR/kWh]	0.085	32
Interest rate	[–]	0.08	–
Life expectancy infrastructure	[y]	20	–

Table B.8: Life cycle assessment indicators used to build the environmental model.

Parameter	Ecoinvent impact
Default operation	
Cement (clinker) production	Cement production, Portland, Europe without Switzerland
Steel and iron production	Steel production, low-alloyed, hot-rolled, RER
Refinery operation	C3 hydrocarbon production, mixture, petroleum refinery operation, Europe without Switzerland,
Waste incineration (plastics)	treatment of waste plastic, mixture, municipal incineration with fly ash extraction, CH
Waste incineration (MSW)	treatment of municipal solid waste, municipal waste with fly ash extraction, CH
Products, operation and installation	
Electricity	market for electricity low voltage, CH
Mining	Limestone quarry operation CH
SiO ₂ , CaCO ₃ , MgCO ₃ (95% credit)	Cement production, Portland, Europe without Switzerland
Ammonium sulfate	market for ammonium sulfate, RER
Ammonia	market for ammonia, anhydrous, liquid, RER
Formic acid	market for formic acid, RER
NaCl	market for sodium chloride, powder, GLO
NaHCO ₃	market for sodium bicarbonate, GLO
Mineralization factory	magnesium factory construction, RoW
Magnetite	magnetite production, GLO
Grinding	rock crushing, RER
Transportation	
Road	market for transport, freight, lorry 16-32 metric ton, RER
Train	transport, freight train, diesel, Europe without Switzerland

C Investment and cost estimation

Figure C.1 illustrates the linear approximation approach for investment costs, following the nomenclature of the MILP formulation.

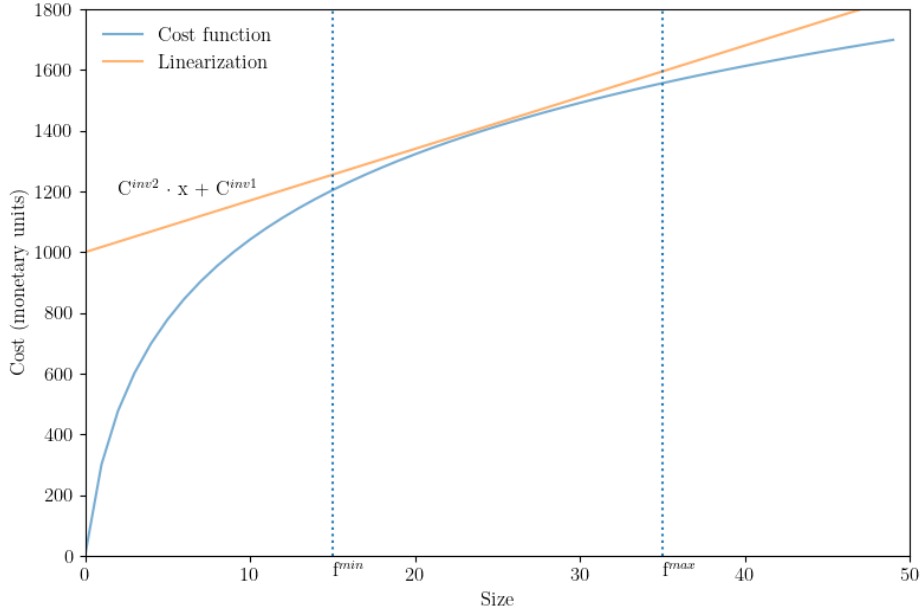


Figure C.1: Linear approximation of the heat exchanger cost function.

C.1 Heat exchanger area and cost

The method here adopted regarding the estimation of the HEX area is an approximation of its true cost, based on the total area of heat transfer and the minimum number of heat exchangers. It is estimated after the optimization procedure and therefore is not embedded in the original MILP formulation. Indeed, the optimization (i.e. minimization) of thermal matches as well as the minimization of the heat exchanger network cost requires a specific mathematical formulation. The problem can be formulated as an MINLP, as extensively discussed in the literature.³³⁻³⁶ However, for the level of detail here required, an approximate value, even if non-optimized, is enough to estimate the contribution of heat exchangers in total cost. Moreover, as further explored, this contribution is typically below 5% of total investment, which validates the approach.

What is known from the combined heat, mass and power MILP formulation is the amount of heat that can be recovered through the design of an adequate heat exchanger network. There is a need to estimate its cost without designing it. By leveraging pinch theory,²² Equation 33 computes the minimum number of heat exchangers, in which $n_{streams}$ is the number of streams, $n_{streams}^{CP}$ is the number of streams that cross the pinch and n_{pinch} is the total number of pinch points.

$$N_{HEX} = (n_{streams} - 1) + (n_{streams}^{CP} - n_{pinch}) \quad (33)$$

The total area required can be estimated using Equation 34, in which Q_i is the heat load of the vertical section (VS) i , $LMTD_i$ is the logarithmic mean temperature difference of the VS i , and $\alpha_{i,j}$ is the heat transfer film coefficient of stream j in the VS i .

$$A_{\text{total}} = \sum_{i=1}^{n_{\text{VS}}} A_i = \sum_{i=1}^{n_{\text{VS}}} \left(\frac{\dot{Q}_i}{LMTD_i} \left(\sum_{j=1}^{n_{\text{streams}}} \frac{1}{\alpha_{i,j}} \right) \right) \quad (34)$$

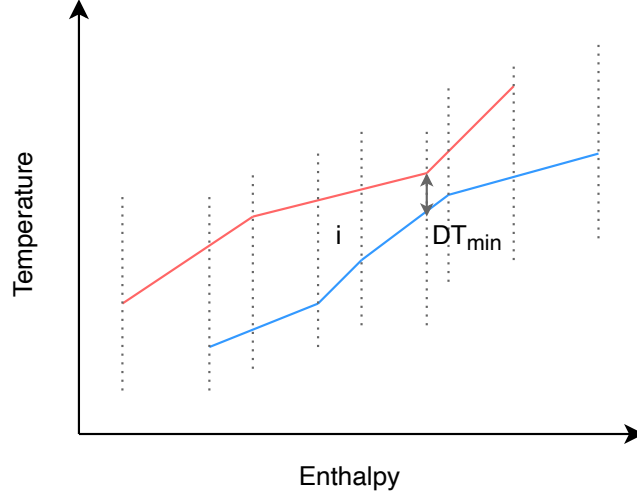


Figure C.2: Area calculation method. i represents of vertical section (VS) between dashed lines, defined by points in which the composite curves slope (i.e. the product between C_p and mass flow) changes. DT_{\min} is the minimum approach temperature.

Further assuming that the total heat exchanger area is equally distributed by all heat exchangers, the mean area of each HEX can be computed according to eq. 35. The incurred cost is computed by using the cost estimation Equations 36 and 37 for shell and tube heat exchangers,²³ and annualized according to Equation 38. Table C.1 summarizes the used parameters.

$$A_{\text{mean}} = \frac{A_{\text{total}}}{N_{\text{HEX}}} \quad (35)$$

$$c^p = \frac{\text{CEPCI}^t}{\text{CEPCI}^{\text{ref}}} \cdot 10^{k_1 + k_2 \cdot \log A_{\text{mean}} + k_3 \cdot (\log A_{\text{mean}})^2} \quad (36)$$

$$c^{gr} = F^{bm} \cdot c^P \quad (37)$$

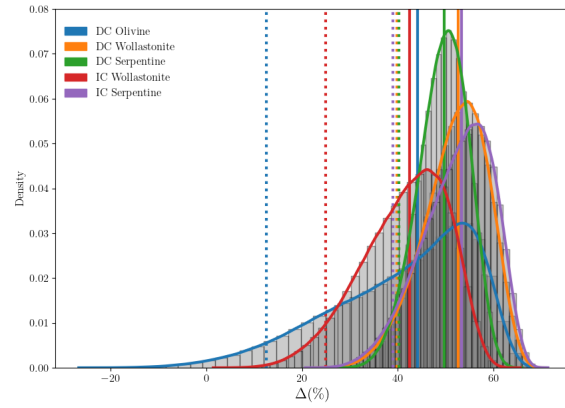
$$c^{int} = F^{an} \cdot c^{gr} \quad (38)$$

As the heat exchange interfaces represent the same energy requirement, changing the interface of one process stream does not make a difference. However, at the unit or site level, where the integration of processes with each other and with the utilities is considered, the heat exchange interface could potentially have a large impact on the overall site heating and cooling demand.

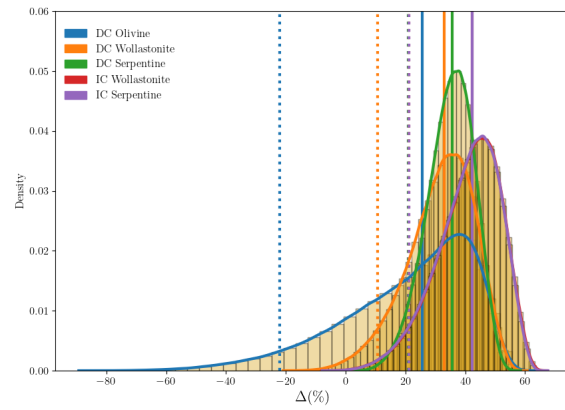
Table C.1: Description of the parameters in the interface cost calculation.

Parameter	Description
A_{mean}	Average area requirement per heat exchanger [m ²]
\dot{Q}_i	Heat load of heat exchanger i [kW]
$\alpha_{i,j}$	Heat transfer coefficient of stream j in vertical section i [kW/m ² K]
LMTD _{i}	Logarithmic mean temperature difference in vertical section i [K]
CEPCI ^t	Cost index at the time the project is realised [-]
CEPCI ^{ref}	Cost index of the reference year [-]
k1, k2, k3	Cost estimation parameters [-]
F^{bm}	Bare module factor [-]
F^{an}	Annualisation factor [1/year]
c^P	Purchase cost [€]
c^{gr}	Grass-roots cost [€]
c^{int}	Annualised cost [€/year]

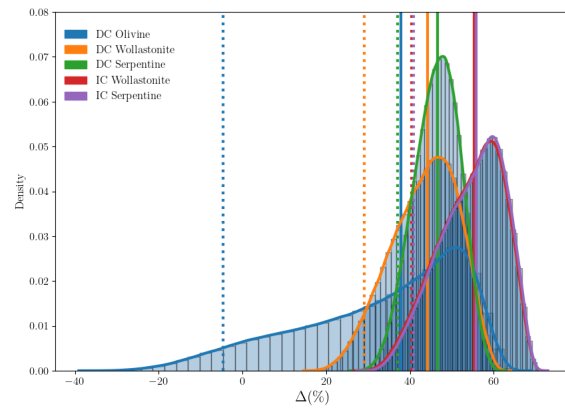
D Results



(a)



(b)



(c)

Figure D.1: Monte Carlo simulation on the relative total cost difference between literature values and total cost of the integrated system for: (a) cement, (b) MSW, (c) steel.

Table D.1: Potential market use of mineralization products (i.e. carbonates), according to Ostovari et al.⁹

Product/Application	Market size	Price (EUR/t)
Fine aggregates on concrete or asphalt	22.5 Gt/y	10
Iron and steel ore	2 Gt/y	60
Blended cement	1 Gt/y	80
Stabilizing hazardous waste	1 Gt/y	100
SiO ₂ as feedstock for glass	58 Mt/y	50
Filler for paper or tire industry	13 Mt/y	350
Nickel feedstock	2 Mt/y	12,000
Pigment on iron oxide or hydroxide	1 Mt/y	142

Carbon footprint analysis

As discussed in the introduction and state-of-the-art, Ostovari et al.^{9,37,38} have extensively studied the use of mineralization for promoting net-negative emissions. Environmental comparison of our approach and the one developed in Ostovari et al.⁹ is provided in Figure D.2, with our results underperforming. There are two main factors justifying such differences:

- Sector-specific integration: In this work, the source of CO₂ is taken into consideration, with the energy needs (and therefore the environmental impact) depending on the point source concentration. Such considerations were overlooked by Ostovari et al..
- Heat integration: The supplementary information section of Ostovari et al. shows thermal energy requirements for which "heat integration has been applied". Therein, it is also assumed that 80% of the sensible heat is recovered from the feedstock after pre-treatment. In this work, rather than relying on such a big assumption, sectors and heat streams were modeled. Heat streams can then be properly integrated.

The differences are not negligible: in the direct carbonation of olivine, a 27% difference in emissions separates both approaches in the steel sector, whereas in the waste sector, the value is close to 35%. It is thus reasonable to suggest that heat integration, characterized by an adequate temperature-enthalpy profile, is an indispensable tool when addressing mineralization, which should not be replaced by assumptions and recovery factors.

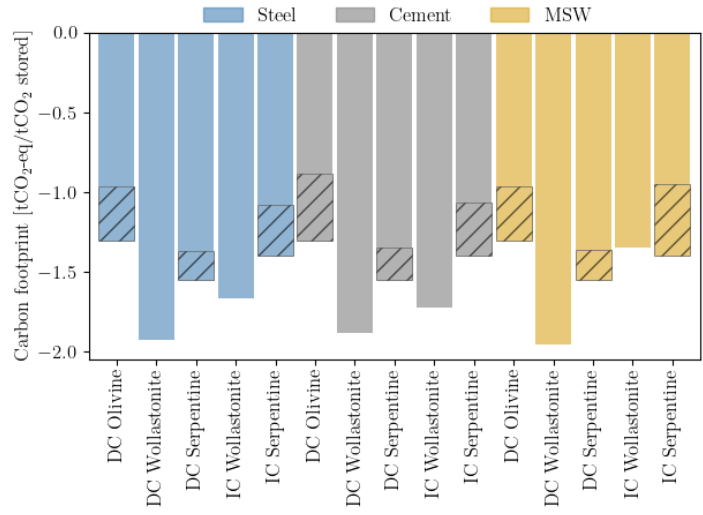


Figure D.2: Comparison of the carbon footprint between this work (plain fill) and the values provided in Ostovari et al.⁹ (hatched bars), upon correction to the same energy mix.

References

- [1] Tock, L. & Maréchal, F. Process design optimization strategy to develop energy and cost correlations of CO₂ capture processes. In Bogle, I. D. L. & Fairweather, M. (eds.) *Computer Aided Chemical Engineering*, vol. 30 of *22 European Symposium on Computer Aided Process Engineering*, 562–566 (Elsevier, 2012).
- [2] Romanov, V. *et al.* Mineralization of Carbon Dioxide: A Literature Review. *ChemBioEng Reviews* **2**, 231–256 (2015).
- [3] Tiefenthaler, J. & Mazzotti, M. Experimental Investigation of a Continuous Reactor for CO₂ Capture and CaCO₃ Precipitation. *Frontiers in Chemical Engineering* **4** (2022).
- [4] Pan, S.-Y., Chang, E. E. & Chiang, P.-C. CO₂ Capture by Accelerated Carbonation of Alkaline Wastes: A Review on Its Principles and Applications. *Aerosol Air Qual. Res.* **12**, 770–791 (2012).
- [5] Snæbjörnsdóttir, S. Ó. *et al.* Carbon dioxide storage through mineral carbonation. *Nat Rev Earth Environ* **1**, 90–102 (2020).
- [6] Chiang, P.-C. & Pan, S.-Y. *Carbon Dioxide Mineralization and Utilization* (Springer Singapore, Singapore, 2017).
- [7] Huijgen, W. J. J., Ruijg, G. J., Comans, R. N. J. & Witkamp, G.-J. Energy Consumption and Net CO₂ Sequestration of Aqueous Mineral Carbonation. *Ind. Eng. Chem. Res.* **45**, 9184–9194 (2006).
- [8] Eikeland, E., Blichfeld, A. B., Tyrsted, C., Jensen, A. & Iversen, B. B. Optimized Carbonation of Magnesium Silicate Mineral for CO₂ Storage. *ACS Appl. Mater. Interfaces* **7**, 5258–5264 (2015).
- [9] Ostovari, H., Sternberg, A. & Bardow, A. Rock ‘n’ use of CO₂: Carbon footprint of carbon capture and utilization by mineralization. *Sustainable Energy Fuels* **4**, 4482–4496 (2020).
- [10] Gerdemann, S. J., O’Connor, W. K., Dahlin, D. C., Penner, L. R. & Rush, H. Ex Situ Aqueous Mineral Carbonation. *Environ. Sci. Technol.* **41**, 2587–2593 (2007).
- [11] Zhang, N., Chai, Y. E., Santos, R. M. & Šiller, L. Advances in process development of aqueous CO₂ mineralisation towards scalability. *Journal of Environmental Chemical Engineering* **8**, 104453 (2020).
- [12] Romão, I., Nduagu, E., Fagerlund, J., Gando-Ferreira, L. M. & Zevenhoven, R. CO₂ fixation using magnesium silicate minerals. Part 2: Energy efficiency and integration with iron-and steelmaking. *Energy* **41**, 203–211 (2012).
- [13] Lackner, K. S., Wendt, C. H., Butt, D. P., Joyce, E. L. & Sharp, D. H. Carbon dioxide disposal in carbonate minerals. *Energy* **20**, 1153–1170 (1995).

- [14] Fagerlund, J., Highfield, J. & Zevenhoven, R. Kinetics studies on wet and dry gas–solid carbonation of MgO and Mg(OH)₂ for CO₂ sequestration. *RSC Adv.* **2**, 10380–10393 (2012).
- [15] Thonemann, N., Zacharopoulos, L., Fromme, F. & Nühlen, J. Environmental impacts of carbon capture and utilization by mineral carbonation: A systematic literature review and meta life cycle assessment. *Journal of Cleaner Production* **332**, 130067 (2022).
- [16] Criado, Y. A., Alonso, M. & Abanades, J. C. Kinetics of the CaO/Ca(OH)₂ Hydration/Dehydration Reaction for Thermochemical Energy Storage Applications. *Ind. Eng. Chem. Res.* **53**, 12594–12601 (2014).
- [17] Kato, Y., Yamashita, N., Kobayashi, K. & Yoshizawa, Y. Kinetic study of the hydration of magnesium oxide for a chemical heat pump. *Applied Thermal Engineering* **16**, 853–862 (1996).
- [18] Ghoorah, M., Dlugogorski, B. Z., Balucan, R. D. & Kennedy, E. M. Selection of acid for weak acid processing of wollastonite for mineralisation of CO₂. *Fuel* **122**, 277–286 (2014).
- [19] Fagerlund, J., Nduagu, E., Romão, I. & Zevenhoven, R. CO₂ fixation using magnesium silicate minerals part 1: Process description and performance. *Energy* **41**, 184–191 (2012).
- [20] Sipilä, J., Teir, S. & Zevenhoven, R. Carbon dioxide sequestration by mineral carbonation Literature review update 2005–2007. Tech. Rep. (2008).
- [21] Maréchal, F. & Kalitventzeff, B. Energy integration of industrial sites: Tools, methodology and application. *Applied Thermal Engineering* **18**, 921–933 (1998).
- [22] Linnhoff, B. & Hindmarsh, E. The pinch design method for heat exchanger networks. *Chemical Engineering Science* **38**, 745–763 (1983).
- [23] Turton, R. *Analysis, Synthesis and Design of Chemical Processes* (Prentice Hall, Boston, MA, 2018), 5th edition edn.
- [24] Ahmad, S., Linnhoff, B. & Smith, R. Cost optimum heat exchanger networks—2. targets and design for detailed capital cost models. *Computers & Chemical Engineering* **14**, 751–767 (1990).
- [25] Pearl, R. & Reed, L. J. On the Rate of Growth of the Population of the United States since 1790 and Its Mathematical Representation1 **6** (1920).
- [26] Villanueva, D. & Feijóo, A. Comparison of logistic functions for modeling wind turbine power curves. *Electric Power Systems Research* **155**, 281–288 (2018).
- [27] Kantor, I. & Santecchia, A. D5.7 – Report on LC assessment tools based on the results of MORE and EPOS. Tech. Rep. (2019).

- [28] Suciu, R.-A. *Fifth Generation District Energy Systems for Low Carbon Cities*. Ph.D. thesis, EPFL, Lausanne (2019).
- [29] Mazzotti, M. Mineral carbonation and industrial uses of carbon dioxide (2005).
- [30] Wernet, G. *et al.* The ecoinvent database version 3 (part I): Overview and methodology. *Int J Life Cycle Assess* **21**, 1218–1230 (2016).
- [31] ENTSO-E. Transparency Platform Restful API - Central Collection and Publication of Electricity Generation, Transportation and Consumption Data and Information for the Pan-European Market. <https://transparency.entsoe.eu/> (last accessed: 24.03.2022).
- [32] Werner, S. EUROPEAN DISTRICT HEATING PRICE SERIES. Tech. Rep. (2016).
- [33] Papoulias, S. A. & Grossmann, I. E. A structural optimization approach in process synthesis—II: Heat recovery networks. *Computers & Chemical Engineering* **7**, 707–721 (1983).
- [34] François, M. & Irsia, B. Synep1 : A methodology for energy integration and optimal heat exchanger network synthesis. *Computers & Chemical Engineering* **13**, 603–610 (1989).
- [35] Grossmann, I. E., Caballero, J. A. & Yeomans, H. Mathematical programming approaches to the synthesis of chemical process systems. *Korean J. Chem. Eng.* **16**, 407–426 (1999).
- [36] Kermani, M., Kantor, I. D. & Maréchal, F. Optimal Design of Heat-Integrated Water Allocation Networks. *Energies* **12**, 2174 (2019).
- [37] Ostovari, H., Müller, L., Skocek, J. & Bardow, A. From Unavoidable CO₂ Source to CO₂ Sink? A Cement Industry Based on CO₂ Mineralization. *Environ. Sci. Technol.* **55**, 5212–5223 (2021).
- [38] Ostovari, H., Müller, L., Mayer, F. & Bardow, A. A climate-optimal supply chain for CO₂ capture, utilization, and storage by mineralization. *Journal of Cleaner Production* **360**, 131750 (2022).